# Genetically Engineered Strains for Combinatorial Cardiovascular Optobiology

Frank K. Lee[1], Jane C. Lee[1], Bo Shui[1], Shaun Reining[1], Megan Jibilian[1], David M. Small[2], Jason S. Jones[2], Nathaniel H. Allan-Rahill[2], Michael R.E. Lamont[2], Megan A. Rizzo[3], Sendoa Tajada[4], Manuel F. Navedo[5], Luis Fernando Santana[4], Nozomi Nishimura[2], Michael. I. Kotlikoff[1]

Department of Biomedical Sciences[1] and Nancy E. and Peter C. Meinig School of Biomedical Engineering[2], Cornell University,
Department of Physiology, University of Maryland School of Medicine[3]
and
Departments of Physiology and Membrane Biology[4], and Pharmacology[5], University of California, Davis School of Medicine

Short Title: Cardiovascular Optobiology

Corresponding Author: Michael Kotlikoff (mik7@cornell.edu)
300 Day Hall
Cornell University
Ithaca, NY 14853

**Abstract**

Rationale: Optogenetic effectors and sensors provide a novel real-time window into complex physiological processes, enabling determination of molecular signaling processes within functioning cellular networks. The effective combination of these optical tools in mice requires designed genetic models that are optically compatible and efficiently assembled. We designed strains for direct biallelic combination, avoiding the multiallelic requirement of Cre recombinase -mediated DNA recombination, focusing on models relevant for cardiovascular biology.

Objective: To address this lack of optogenetic resources by combining lineage-specific expression of optogenetic effectors and sensors in single mouse lines and demonstrating their utility.

Methods and Results: Twenty-two lines of mice were created in which optogenetic effectors (11 lines) or $Ca^{2+}$ sensors (11 lines) were expressed in a lineage-specific manner in cardiac pacemaker cells (SAN), cardiomyocytes, vascular endothelial and smooth muscle cells, as well as other cell types. We show functional responses associated with optical formation of the second messengers $InsP_3$ (opto$\alpha$1AR) and cAMP (optoß2AR), or $Ca^{2+}$-permeant membrane channels (CatCh2), in targeted cells in these mice. Green (GCaMP5, 8 and 8.1) and red (RCaMP 1.07) $Ca^{2+}$ sensors were chosen to enable simultaneous fluorescent detection of cellular responses. Biallelic crosses were created with robust expression of sensor/effector pairs. We present examples of novel *in vivo and ex vivo* experiments in selected strains including cardiac pacing with stimulation of HCN4 conduction cells, intravital cardiac imaging of GCaMP8 with two-photon microscopy, optical vascular dilation/constriction by smooth muscle (Acta2) and vasodilation by light activation of endothelium (Cdh5). These experiments highlight the potential of these mice to uncover new insight into mechanisms regulating cardiovascular function.

Conclusions: These new mouse lines efficiently express optical effectors and sensors in heart, blood vessels, and other tissues and can be efficiently combined enable novel *in vivo* and *ex-vivo* studies and can be combined or crossed with relevant cardiovascular disease models, constituting a new toolbox for cardiovascular biology.

Keywords: calcium imaging, optogenetics, imaging

## Introduction

Optogenetic effectors and sensors enable the interrogation of complex biological signaling networks at the molecular level *in vivo*[1-5]. The power of these molecular tools is optimized in mammalian systems by genetic lineage specification and combinatorial strategies. The former provides the ability to activate or determine the responses of individual cellular components of a complex network, whereas the latter, using spectrally compatible optogenetic tools, enables the dissection of the network by activation of defined elements and simultaneous interrogation of individual system component responses, thereby significantly enhancing the ability to understand functional networks. Although simple in concept, the usefulness of optogenetic tools in mammalian systems requires a parsimonious allelic strategy that minimizes experimental crosses, while supporting robust and consistent sensor/effector expression. For example, while DNA recombination strategies can achieve lineage specificity by crossbreeding Cre recombinase and floxed responder mouse lines[6], the attendant allelic requirements render this approach impractical for combinatorial experiments using multiple optogenetic tools. Such experiments are facilitated by the design and assembly of sets of individual mono-allelic lines that strategically place spectrally distinct optogenetic effectors and sensors in interacting cell lineages, allowing simple crosses to probe cell-cell signaling. Here we report a marked expansion of the mammalian optogenetic toolbox through the development of multiple mouse lines designed for combinatorial experiments within the cardiovascular system. Interacting vascular, neural, and muscular tissues are targeted through a variety of genetic strategies, expression specificity confirmed, and examples of their use provided.

# Methods

## Construction of transgenic strains

Mouse lines were created by injection of either homologously recombined bacterial artificial chromosomes (BACs)[7], or previously established promoter constructs with desired effector or reporter, into fertilized single cell eggs. All constructs are listed in Supplemental Materials, Table S1. The optogenetic effector strains contained either opto$\alpha$1AR[8], optoß2AR[8], or CatCh2[9] genes linked to downstream IRES-LacZ for simple identification of transgene expressing strains. The reporter strains contained either EGFP- or RFP-derived GECIs as single fluorophores (GCaMP8/8.1 or RCaMP1.07) or a fusion protein of green and red fluorophores (GCaMP8.1-mVermilion or GCaMP5-mCherry). BAC transgenes were constructed by homologous recombination to position the desired transgene inframe with the initiation codon of the native gene as previously described [7]. Purified BAC transgene plasmids were microinjected into single-cell embryos at the Cornell University Transgenic Core Facility or the UC Irvine Transgenic Mouse Facility. Pups were screened for the desired transgene by PCR analysis using primers listed in Table S1, backcrossed to C57Bl/6J and further screened by immunohistochemistry, Xgal staining, or fluorescence imaging using standard methods. Briefly, tissues were either fixed overnight in 4% paraformaldehyde (PFA) at 2-8°C, rinsed in 1x phosphate-buffered saline (PBS) and equilibrated in 30% sucrose/1x PBS at 2-8°C (for immunohistochemistry), or fixed for 2 hrs in 4% PFA on ice and processed to 30% sucrose (for Xgal staining). Anti-GFP or anti-dsRed antibodies were used as previously described[10]. For fluorescence imaging, sections were washed three times in 1X PBS, mounted with VectaShield with DAPI (Vector Laboratories), and imaged using a Leica DMI6000B inverted microscope. Monochrome images were colorized using ImageJ software as described in Supplemental Methods.

## Imaging and stimulation

*Ex-vivo* arterial imaging: Freshly isolated mid cerebral arteries were cannulated on glass pipettes mounted in a 5 mL myograph chamber and pressurized as described previously[11], and only arteries that constricted more than 30% to isosmotic physiological salt solution containing 120 mM KCl were used. Optogenetic effector proteins were

activated at 473 nm using in an Olympus FV1000 microscope with a SIM scanner, which enables photostimulation. To avoid unintended activation of genetic proteins by ambient light, the isolated vessels were kept in the dark or under red light. Arterial diameter was determined from stacks of tiff images using the Myotracker video-edge detection plugin in ImageJ[12].

*Ex vivo* heart imaging: Mice were given 100U of heparin IV immediately prior to euthanasia. The heart was quickly excised in cold Tyrode's buffer, cannulated, and perfused with Tyrode's buffer (37°C, equilibrated with 95% $O_2$/5% $CO_2$). Optogenetic stimulation of the SA nodal region was as described below. GCaMP8 fluorescence was captured using an Andor-iXon CCD camera mounted on an Olympus MVX10 fluorescent microscope (ex: 472/30 nm, em: 520/35 nm).

*In vivo* heart stimulation**:** Mice were anesthetized with ketamine (100 mg/kg) and xylazine (10 mg/kg) via intraperitoneal injection, intubated with a 22-gauge cannula, ventilated (95 breath/min, 12 cm $H_2O$ end-inspiratory pressure; CWE SAR-830/P ventilator), and maintained on 1.5% isoflurane. 5% glucose (0.1 mL/10 g) and atropine sulfate (5 µg/100 g body weight) were injected subcutaneously and body temperature was maintained at 37.5°C with a heating pad. The heart was surgically exposed by dissection of the sternum and diaphragm, and ribs retracted for optical access to the thoracic cavity. For optical stimulation of the SA-node, mice were positioned on their back on a stereotaxic stage, the pericardial sac was removed, and the thymus gland repositioned from covering the right atrium. Illumination of the node was performed using a 105-µm core fiber (Thorlabs) coupled to a 473-nm continuous wave, diode-pumped solid-state laser system (Opto Engine LLC; BL-473-00200-CWM-SD-03-LED-F). The tip of the laser fiber was inserted through 500-µm metal tubing and clamped within a four-way axis micromanipulator that allowed positioning of the fiber tip on the anterior junction of the right atrium and superior vena cava. For stimulation of the left ventricle free wall, mice were positioned on their right side and a left thoracotomy was performed between ribs 7 – 8 to gain access to the heart. The tip of the optical fiber was coupled to a collimating lens mount that was positioned to direct the beam at the

left ventricle. A customized titanium probe affixed to the stereotaxic stage was adhered (Vetbond) to the left ventricle free wall to minimize movement associated with respiratory and cardiac contractions. Electrocardiogram (ECG) electrodes were attached to 21-gauge needles inserted subcutaneously through the front and contralateral hind limb and recorded with an isolated differential amplifier (World Precision Instruments; #ISO-80). ECG and lung pressure traces were continuously monitored through an oscilloscope. Laser pulses were controlled through a TTL signal delivered by a function generator (Agilent 33210A) and signals digitized and recorded on a computer using MATLAB.

*In vivo* 2-photon imaging: A left thoracotomy was performed as above and a 3D-printed titanium stabilization probe with imaging window[13, 14] attached to the left ventricle free-wall using tissue adhesive (Vetbond). Texas-Red conjugated 70-kDa dextran (3% in saline; Thermo Fischer Scientific #D1830) was injected retro-orbitally to identify the vasculature. A Ti:Sapphire laser (Chameleon, Coherent) with wavelength centered at 950 nm was used to excite indicator molecules and images collected using a custom multiphoton microscope equipped with four detection channels and high-speed resonant scanners running ScanImage[15]. Emission fluorescence was detected using long-pass dichroic mirrors and bandpass filters for GCaMP8 (517/65 nm) and Texas-Red (629/56). Water was placed within a rubber O-ring of the stabilization probe to allow immersion of the microscope objective (Olympus XLPlan N 25x 1.05 NA). ECG and respiratory signals were collected while imaging z-stacks (50-100 frames; 2 μm per z-step; 30 frames/sec) in 4 – 5 different regions in each mouse. Image reconstruction was performed as previously described[13], by indexing image lines based on their acquired position within the cardiac or respiratory cycles. Additional analysis is described in Supplemental Methods.

*In vivo* arterial imaging: Mice were anesthetized with 5% isoflurane, maintained with 2% isoflurane using a nose cone, and placed on a heated stage. The cremaster or femoral vessels were visualized and superfused with warm PSS equilibrated with 95% $O_2$-5% $CO_2$ [16]. Endothelial cells of either cremaster or femoral vessels were stimulated with a

473-nm, continuous wave, diode-pumped solid-state laser system (Opto Engine LLC; BL-473-00200-CWM-SD-03-LED-F) at power and pulse length as specified. Optical fiber coupled to a collimating lens was attached to a 3-axis micromanipulator and positioned to aim the light at the desired vessel. To quantify arterial diameter changes, vessels were illuminated with white light. Raw images from the Andor-iXon camera were converted to tif files using ImageJ. Motion artefacts between frames were removed using MATLAB's Image Processing Toolbox prior to vessel analysis. Each frame was translated to maximize the 2-dimensional correlation with respect to the first frame using the function *imregcorr*. This correlation was calculated in an area of the images not affected by light leakage from the stimulation laser in order to avoid stabilizing on the beam rather than the tissue structure. Once the image was stabilized, vessel width and sidewall intensity were measured as a function of time across each frame. MATLAB was used to interpolate the intensity profile along a user-specified line across a vessel using the *interp2* function. To improve the resulting profile, intensity was averaged over 28.05 μm. The two peaks in the profile were recorded as the sidewall intensities and the distance between the peaks recorded as the vessel width. If the profile still included significant noise, a quadratic fit was performed around each peak to find a more accurate peak location and intensity.

Patch-Clamp Electrophysiology: All current recordings were acquired at room temperature using an Axopatch200B amplifier and a Digidata1440 digitizer (Molecular Devices, Sunnyvale, CA). Borosilicate patch pipettes were pulled and polished to resistance of 3-6 MΩ for all experiments using a micropipette puller (model P-97, Sutter Instruments, Novato, CA). Freshly dissociated arterial myocytes were kept in ice-cold $Mg^{2+}$-PSS before being recorded.

Voltage-gated $K^+$ ($I_K$) and light-activated CatCh2 ($I_{Cat}$) currents were recorded using conventional whole-cell configuration of the voltage-clamp technique. Currents were recorded at a frequency of 50 kHz and low-pass filtered at 2 kHz. $I_K$ and $I_{Cat}$ were recorded while cells were exposed to an external solution composed of 130 mM NaCl, 5 mM KCl, 3 mM $MgCl_2$, 10 mM Glucose, and 10 mM HEPES adjusted to 7.4 using

NaOH. The pipette solution was composed of 87 mM K-Aspartate, 20 mM KCl, 1 mM $CaCl_2$, 1 mM $MgCl_2$, 5 mM MgATP, 10 mM EGTA, and 10 mM HEPES adjusted to 7.2 by KOH. A liquid junction potential of 12.7 mV was corrected offline. $I_K$ were activated by a series of 500 ms test pulses increasing from -70 mV to +60 mV. $I_{Cat}$ was recorded while cells were held at -70 mV before and after exposure to 488 nm light.

## Results

We report the generation of CHROMus$^{TM}$ mice, 22 lines of optogenetic sensor and effector mice, in which the expression of the transgene is lineage specified (Table S1), and demonstrate the utility of these lines for *in vivo* and *ex vivo* imaging. The optogenetic effector proteins we selected for this toolbox were opto$\alpha$1AR[8], opto$\beta$2AR[8], and CatCh2[9]for light activation of cAMP or IP3 secondary messenger pathways or $Ca^{+2}$ membrane channel, respectively. Each of the open reading frames for the optogenetic proteins were linked to an IRES element and bacterial LacZ ORF for simple screening. The fluorescent GECI proteins, GCaMP and RCaMP, in our reporter strains were derived from circularly permutated EGFP and RFP constructs for *in vivo*, real-time reporting of cellular $Ca^{2+}$ signaling (Figure S1).

CHROMus$^{TM}$ mice can be used directly as individual optogenetic effector or fluorescent reporter strains to study real-time response to light activation of the target tissue or to study cellular or subcellular $Ca^{2+}$ signaling in response to various physiological stimuli. However, the system provides the novel opportunity to create novel effector/reporter combination strains to study the complex network of physiological signals and responses, as illustrated in Figure 1. Here, activation of the CatCh2 protein expressed in SA nodal pacemaker cells triggers cardiac conduction, as monitored by GCaMP8 fluorescence in ventricular myocytes. Other combinatorial preparations from the CHROMUS$^{TM}$ toolbox enable the evaluation of cellular function in healthy or diseased animal models. We have constructed 11 strains expressing various optogenetic effector proteins in 7 different lineages and 11 strains expressing fluorescent GECI reporter proteins in 7 lineages across a wide range of tissues, organs, and systems (Table S1).

### ***Cardiac Conduction System Optogenetic Mice***

The potassium/sodium hyperpolarization-activated cyclic nucleotide-gated channel 4 protein (HCN4) underlies the pacemaker current in the sinoatrial (SA) node, controlling heart rate and heart rhythm[17, 18]. For light-activated control of heart rhythm, we constructed a HCN4$^{BAC}$-CatCh2_IRES_LacZ strain, where the expression of the opto-effector CatCh2 and a marker protein (LacZ) are under transcriptional control of a

bacterial artificial chromosome (BAC) containing the HCN4 locus, thus directing expression to the cells of the cardiac conductance system. X-gal staining of adult HCN4$^{BAC}$-CatCh2/LacZ mice demonstrated specific staining in cells of the cardiac conductance system, including the sinoatrial node region in the right atrium, the atrioventricular junction, and the ventricular conducting network (Figure 2A). LacZ expressing cells were observed at the base of the right carotid vein where it joins the right atrium (Figure S2A) and along the right carotid vein to the base of the common carotid vein (Figure S2B). Expression was also documented in embryonic (E10.5) and neonatal (PN4) hearts in the atrium and the ventricular conducting system (Figure 2B).

To confirm optical control of heart rhythm, we stimulated the SA node area with 473-nm light *in vivo* while recording the ECG. As shown in Figure 2C, cardiac conduction was driven with stimulation between 2Hz and 4Hz, with dropouts at higher frequencies. Heart rhythm returned to normal following optical stimulation (Figure S2C), and illumination of off-target tissue (left ventricle) did not result in optical rhythm control (Figure S2D). Pacing was maintained with laser pulse lengths varying between 15 and 70 ms (data not shown). ECG parameters indicated R-wave duration and PR interval increased significantly, relative to the autonomously activated cardiac cycle (Figures 2E, 2G). The increase in laser-stimulated R-wave duration is shown as a widening of the R-wave in the R-wave-centered average of ECG for stimulated and unstimulated beats and the extended PR interval in the P-wave-centered average of ECG sections (Figures 2D, 2F).

To demonstrate the feasibility of combining optogenetic effector and sensor lines, we crossed HCN4$^{BAC}$-CatCh2/LacZ and αMHC-GCaMP8 strains. Pacing by laser stimulation resulted in coupling between optical stimulation and GCaMP8 fluorescence, as shown in Figure 2H, and the supplemental movie SM1. Differences in effector and sensor kinetics must be considered at high stimulation rates, as previously reported[19]. The HCN4$^{BAC}$-CatCh2 strain can also be mated to Acta2$^{BAC}$-GCaMP5_mCherry (Figure 4) and Cdh5$^{BAC}$-GCaMP8 lines (Figure 5) to study smooth muscle or endothelial cell responses to the cardiac pacing.

For the study of the development of the cardiac conduction system and disturbances of conduction in disease states, we developed a HCN4$^{BAC}$-GCaMP8 mouse line. GCaMP8 is expressed in the *sinus venosus* (Figure 2I, left panels) of the embryonic heart and in the SA nodal area at the junction of right atrium and right carotid vein in the adult heart, extending down to the base of the common carotid artery (Figure 2I, right panel), similar to the expression pattern in HCN4$^{BAC}$- CatCh2 strain (Figure S2B). In developing embryos, spontaneous GCaMP8 signaling was observed in the embryonic heart at embryonic day (ED) 8.5, 10.5, and 13.5, as well as in the neonatal heart at post natal day 4 (Figure S3A). Conduction of the GCaMP8 fluorescence signal was observed moving from the atrium to the ventricle in the E13.5 embryo (Movie SM2). In the adult heart, GCaMP8 signaling was observed prior to spontaneous ventricular contractions (Figure S3B, Movie SM3).

***Cardiac Myocyte Optogenetic Mice***

We constructed two optogenetic strains designed to study $Ca^{2+}$ signaling and electrical communication between heart cells ($\alpha$MHC-GcaMP8), using a minimal promoter for $\alpha$MHC protein[20]. In order to optically initiate cardiac dysrhythmias at virtually any surface region of the heart, we developed the $\alpha$MHC-CatCh2_IRES_LacZ strain, which expresses the CatCh2 and LacZ transgenes in cardiomyocytes. X-gal stained cryosections of the heart showed widespread staining of throughout the heart (Figure 3A). Laser irradiation (473 nm) of the left ventricle enabled the stimulation of ventricular premature activations at lower frequencies, and complete ventricular pacing at 8 Hz; above 8 Hz pacing was lost but irregular ventricular initiation could be produced, consistent with the refractory period of ventricular myocytes (Figure 3B). As predicted for ventricular activation, the ECG showed markedly enhanced QRS duration without corresponding P-waves, as visualized in an R-wave-centered average of ECG sections for stimulated and unstimulated beats in three mice (Figure 3C). Differences in ECG morphology among animals at baseline, as well as unsuccessful stimulation for some beats accounts for high variability and abnormal morphology in the averaged trace. The mean R-wave duration significantly increased upon laser stimulation compared to the

native unstimulated heart beat in all three mice examined (Figure 3D). Higher magnification ECG traces of autonomous heart activation following ventricular laser stimulation show typical widened QRS complexes (red) followed by return to normal heart activation (Figure 3E, 3F).

As described above, we also created the αMHC-GcaMP8 line to enable visualization of *in vivo,* real-time, cardiac $Ca^{2+}$ responses under different experimental stimuli and disease conditions. Cryosections from the heart revealed widespread GCaMP8 fluorescence and immunoreactivity in hearts from this strain (Figure 3G). To obtain high resolution intravital images of a beating heart, we injected Texas Red-conjugated dextran retro-orbitally to label the vasculature and acquired two-channel, two-photon images of the left ventricle (Figure 3H). GCaMP8 $Ca^{2+}$ fluorescence was observed in cardiomyocytes in the stabilized ventricular free wall during the normal cardiac cycle, coincident with heart contractions. The vascular dextran fluorescence signal reports only motion-related fluorescence changes (Figure 3I, Movie SM4).

***Smooth Muscle Optogenetic Mice***

We constructed optogenetic effector and sensor BAC transgenic mice using transcriptional activity from a region that spanned the smooth muscle specific α-Actin2 gene, which is selectively expressed in smooth muscle[21]. Sensor strains expressing GCaMP (5 or 8.1) and RcaMP1.07 (15) fluorescent $Ca^{+2}$ reporters, and effector strains expressing the optoα1AR[8], optoß2AR[8], and CatCh2[9] proteins, were developed under smooth muscle specific transcriptional control.

We engineered three recombinant BAC constructs to drive expression of red or green-red sensors in smooth muscle cells (see Figure S1). The $Acta2^{BAC}$-RcaMP1.07[22] strain expresses the sensor selectively in arterial smooth muscle (Figure S4A, upper panels). *In vivo* imaging revealed cyclic fluorescence increases associated with contractions of the right atrium (Figure S4A, lower panel, SM5). When used with optoeffector mice, the line eliminates spectral overlap with excitation of GFP -based sensors.

Acta2$^{BAC}$-GcaMP5_mCherry mice provide the advantage of ratiometric $Ca^{2+}$ determination, as well as ease of expression determination *in vivo.* As shown in brain surface vessel images (Figure 4A upper panel), the GCaMP5-mCherry fusion protein is strongly expressed in the arterial system extending to the arteriolar-capillary junctional cells, but not in the capillary network. To further enhance intensity of red fluorescence, we created a second dual color sensor line using the same transcriptional strategy, but substituting mVermilion, a novel monomeric mCherry variant with a two-fold increase in brightness but equivalent excitation and emission profiles. The Acta2$^{BAC}$-GcaMP8.1_mVermilion displayed a similar expression pattern (Figure 4A – lower panel). *In vivo* experiments with these lines indicated robust smooth muscle $Ca^{2+}$ dependent fluorescence. Contractions of blood vessels, airways, and gastrointestinal organs demonstrated increases in green fluorescence during muscle contraction. As shown in Figure S4C and movie SM6, *in vivo* fluorescent imaging of spontaneous contractions in the large intestine showed a wave of GcaMP5 signaling in the longitudinal muscles that was coupled to contractions, whereas mCherry fluorescence remained constant (data not shown).

We constructed three effector strains for smooth muscle optical activation using the ACTA2 BAC (RP23-370F21; Table S1) and examined the expression of the LacZ protein located downstream of the optogenetic effector coding sequence in different tissues from Acta2$^{BAC}$-Opto$\alpha$1AR_IRES_lacZ, Acta2$^{BAC}$-Optoß2AR_IRES_lacZ and Acta2$^{BAC}$-CatCh2_IRES_lacZ by X-gal staining. The staining data shows widespread expression of all 3 constructs in the brain arterial system (Figure 4B), including the arteriolar/capillary junction. LacZ activity was also observed in arteries supplying the diaphragm, smooth muscles surrounding coronary blood vessels, the bladder, the bladder, bronchiolar and vascular smooth muscles of lung, the small intestines (Figure S4B), and other tissues such as kidney and uterus (data not shown). X-gal staining of a non-transgenic littermate did not detect LacZ activity (Figure S4B).

As smooth muscle contraction and relaxation is often mediated by receptor -mediated activation of phospholipase C or adenylyl cyclase and associated increases in InsP3 or

cAMP, respectively, we examined constriction or dilation of isolated cerebral arteries in response to optical activation of the chimeric optoα1AR and optoß2AR proteins. Brief exposure of arteries isolated from Acta2$^{BAC}$-Optoα1AR_IRES_lacZ mice to 405nm light resulted in vasoconstriction (Figure 5A, left panel), while light -activated arteries from Acta2$^{BAC}$-Optoß2AR_IRES_lacZ lines underwent slow dilations (Figure 5A, middle panel; Movie SM7), demonstrating functional expression of the proteins and expected physiologic responses. The activation of channelrhodopsin in arteries isolated from Acta2$^{BAC}$- CatCh2_IRES_lacZ mouse resulted in rapid constriction (Figure 5A, right panel; Movie SM8).

Optoeffector coupling was demonstrated at a cellular level in whole-cell, voltage clamped arterial myocytes. We first examined coupling through the known linkage between cAMP/Protein Kinase A signaling and voltage-gated potassium channels in arterial myocytes [23-26]. Macroscopic $I_K$ currents from single voltage-clamped myocytes isolated from male mesenteric and mid-cerebral arteries were recorded before and after photo-activation of optoβ2. $I_K$ (composed of Kv1, Kv2.1, and BK currents) was activated at 10 s intervals by the application of a 500 ms step depolarization from the holding potential of -70 mV to +60 mV. Exposure to 488 nm light to activate the optoß2 protein increased the amplitude of $I_K$ 10 s after the activation of optoβ2, reaching a higher, relatively stable plateau approximately 80 s after photoactivation (Figure 5B). Although the dispersion of $I_K$ amplitudes increased about 150 s after activation of optoβ2, $I_K$ remained higher than under control conditions for at least 500 s. Exposure to a second and third pulse of light had limited additional effects, suggesting that the initial optoβ2-induced potentiation of $I_K$ was near maximal. In five similar experiments in mesenteric myocytes, optoβ2 photoactivation increased $I_K$ 1.15 ± 0.04-fold at +60 mV, and 1.23 ± 0.05-fold in cerebral arterial myocytes.

Similarly, CatCh2 optical activation was examined in cerebral and mesenteric arteries by recording membrane currents at -70 mV before and after illumination (488 nm, 50ms pulses at 1 Hz). As shown in Figure 5C, optical stimulation repeatedly evoked fast inward currents that terminated as soon as the laser was turned off. In the

representative cerebral myocyte shown, the amplitude of the evoked current was about 75 pA, and subsequent light pulses evoked stable $I_{CatCh}$ with an amplitude of 68 ± 1 pA, suggesting that under our experimental conditions there is a relatively small level of inactivation of CatCh2 channels (Figure 5C, upper panel). Longer light pulses produced a larger inward current (~125 pA) that quickly (~100 ms) decayed to a lower amplitude (~35 pA) plateau, remaining relatively constant as long as the laser was turned on. This $I_{Cat}$ quickly terminated (<100 ms) after the laser was turned off. Notably, a second 488 nm light pulse to the same cell evoked an $I_{Cat}$ that lacked the high-amplitude transient component of the first light pulse but had the amplitude and kinetics of the steady-state $I_{Cat}$ in the first pulse. Similar observations were made in isolated mesenteric myocytes (Figure 5B, middle panels). The activation of cerebral myocytes resulted in higher currents compared to mesenteric arteries and repeated pulses resulted in dampened initial inward current (Figure 5B, bottom panels). Thus, ACTA2 optoeffector lines express functional chimeric receptors and channel proteins, enabling optical modulation of smooth muscle signaling in a variety of experimental conditions.

***Endothelial Optogenetic Mice***

To enable studies of the interactions between endothelium and surrounding perivascular cells we created three BAC transgenic optogenetic effector, and one fluorescent reporter, mouse lines using the endothelial cell specific cadherin5 gene locus. As with smooth muscle, Opto$\alpha$1AR, Optoß2AR, and CatCh2 cDNAs and LacZ cDNAs were targeted to the Cdh5 initiation codon, with an IRES and the LacZ sequence downstream of the optoeffectors. X-Gal staining revealed wide expression in endothelial cells of the heart (Figure 6A), brain (Figure S5A), and other tissues (Figure S5B). Similarly, GCaMP8 selective expression in endothelial cells was achieved in $Cdh5^{BAC}$-GCaMP8 mice (heart and brain shown, Figure 6B, S5C). Endothelial GCaMP8 signal was sufficiently bright to be observed in coronary microvasculature using intravital 2-photon microscopy (Figure 6C).

To confirm functional expression of optoeffector proteins, we deployed several analyses. First, we examined endothelium -induced vasodilation that occurs secondary

to the release of $Ca^{2+}$ in and synthesis of NO in EC[27]. Optical activation of femoral arteries in $Cdh5^{BAC}$-Opto$\alpha$1AR_IRES_LacZ mice *in vivo* resulted in marked vasodilation, whereas laser stimulation alone caused a slight vasoconstriction in control arteries (Figure 7A). Similar results were obtained in cremaster arteries, but not in control arteries (Figure S5D). We also examined the propagation of arterial dilation that occurs following muscarinic stimulation[28], and is difficult to separate from agonist diffusion[29]. Laser stimulation triggered bidirectional arterial dilation at points distal to the laser beam, with a delay in the onset of vasodilation and attenuation of the amplitude (Figure 7B). Vasodilation was triggered at 32.2mW, but not at lower laser powers (Figure 7C). Photoactivation of chimeric ß2 adrenergic receptors in Optoß2AR mice also triggered vasodilation (Figure 7D). Interestingly, ß2AR -mediated dilation did not result in conducted dilation distal to the point of laser stimulation as observed in opto$\alpha$1AR mice.

***Other Optogenetic Lines***

The gap junction protein connexin40 is expressed in specialized cells of the cardiac conduction system and in arterial endothelial cells, and expression in embryonic myocytes is critical for heart function prior to development of a mature conduction system[30]. To facilitate improved studies of embryonic and adult cardiac conduction defects, as well as physiologic vasomotor control, we created a $Cx40^{BAC}$-GCaMP5_mCherry mouse line. The ratiometric green-red fusion protein is expressed in arterial endothelia from the kidney, the ventricular conductance system and atrial myocytes (Figure 8A), and in arterial endothelial cells (Figure S6A). To extend studies to the sympathetic nervous system, we used the dopamine ß-hydroxylase locus to target optogenetic effectors to peripheral neurons and adrenal medulla cells (reviewed in Gonzalez-Lopez and Vrana, 2019[31]). X-gal staining of adult brain and adrenal glands of $Dbh^{BAC}$-CatCh2_IRES_lacZ demonstrated the expression of LacZ in the *locus coeruleus* (Figure 8B) and adrenal medulla (Figure S6B). BAC DNA from the aldehyde dehydrogenase family 1 L1 (Aldh1L1) gene locus was similarly used to target glial cells. $Aldh1L1^{BAC}$-Opto$\alpha$1AR_IRES_LacZ mouse express in cerebellar (Figure 8C) and olfactory regions in the brain and the kidney (Figure S6C). We constructed the SP-

$C^{BAC}$-GCaMP8 mouse to target reporter expression in Type II alveolar cells. Anti-GFP antibody analysis of lung sections indicated wide distribution of GCaMP8 expression (Figure S6D).

## Discussion

We have generated 22 lines of optogenetic sensor and effector mice, in which the expression of the optogene is lineage specified in cardiovascular and related cell lineages (Table S1), and sensor/effector pairs can be combined through simple, monoallelic crosses. More broadly, the lines facilitate the combination of two technologies, each with enormous potential for use in the dissection of signaling processes in complex multicellular systems: genetically encoded optical sensors[1, 2, 32] and effectors[3]. Individually, these technologies have advanced our understanding of physiological *in vivo* processes; combined, biallelic effector/reporter strains constitute a novel platform for the activation and detection of cellular signaling *in vivo*. These new strains comprise a publicly available molecular toolbox that enables investigators to generate physiologically relevant mono- or multiallelic transgenic strains tailored to their research interests, without the need for requisite technical expertise and financial commitment associated with constructing transgenic strains. The monoallelic nature of these lines also facilitates crosses with mouse models of cardiovascular disease. All strains are available as part of a collaborative effort between Cornell/National Heart Lung Blood Resource for Optogenetic Mouse Signaling (CHROMus™) and The Jackson Laboratory.

Previous approaches have developed, or exploited available, *Cre recombinase* driver mice to confer tissue specific expression of fluorescent markers or optogenetic sensors downstream of LoxP-STOP-LoxP sequences[6, 33]. While this approach has the advantage of using previously characterized Cre lines and can use strong promoter sequences to drive optogenetic protein expression, there are several important drawbacks to this approach. These include variable penetration of the Cre-mediated recombination at LoxP sites within the target cells, limited specificity of non-BAC Cre

promoters[33], and the inefficient process of producing bi-allelic mice for experiments. The latter drawback excludes, for practical purposes, one of the most important advantages of the use of optogenetic mice – crosses with genetic strains or mutant lines that mimic human disease. The use of Cre/Lox approaches for such experiments requires complicated and inefficient breeding strategies. The strains reported here provide direct, tissue -specific expression of optogenetic proteins and enable simple mating strategies for the development of biallelic mice.

Separate targeting of cardiac conducting cells and myocytes enabled light-activated heart activation, and we demonstrate activation of the heart either through stimulation of cells within the AV node (Figure 2), or extra-conduction system activation equivalent to premature ventricular contractions (Figure 3). By crossing nodal optoeffector (HCN4$^{BAC}$-CatCh2/LacZ) and myocyte sensor ($\alpha$MHC-GCaMP8 strains) mice, we demonstrate the feasibility of combinatorial optogenetics and report the ability to activate and detect heart signaling non-invasively (Figure 2H, and the supplemental movie SM1). We also demonstrate the ability to selectively examine cardiac conduction using HCN4$^{BAC}$-GCaMP8 mice, and their robust signaling of conduction events in embryonic, neonatal, and adult hearts (Figure 2). The cardiac GCaMP8 sensor lines represent several improvements, as they exploit recent structure-based improvements in circular permutation of GFP[34, 35], resulting in higher brightness and dynamic range. Conduction failures result in the implantation of more than 200,000 pacemakers annually in the United States alone[36], and the ability to selectively initiate cardiac conduction at local sites within the heart (optoeffector lines), either through activation of specialized conducting cells or myocytes, and to monitor activation of the conduction system (optosensor lines), confers significant experimental advantages both in understanding conduction system failure and strategies to develop biological pacemakers[37-39]. Similar approaches can be envisioned for studies of heart failure, a major cause of mortality world-wide[40]. Two areas of specific value would be the understanding of cardiomyopathy induced arrhythmias[41] and cell and gene-based approaches to therapy[42].

The development of mouse lines with robust expression of optical effectors and sensors in smooth muscle and endothelial cells provides similar experimental advantages for vascular biology. We report the first mice conferring lineage specific expression of sensors that allow light activated depolarization through CatCh2 channels or release of intracellular $Ca^{2+}$ through Opto$\alpha$1AR, chimeric $\alpha$- adrenoceptors, as well as relaxation of smooth muscle through photoactivation of Optoß2AR, chimeric ß2 receptors. Interestingly, we observed rhythmic endothelial cell signaling during the cardiac cycle, enabling dissection of mechanisms that regulate blood flow, matching perfusion to metabolic demand[43]. Similar approaches have led to important advances in the understanding of metabolic vascular coupling in the brain and other arterioles[44-46], but studies in the heart face additional imaging challenges associated with imaging the beating heart. We present both mechanical (Fig 2) and deconvolution (Fig 3) approaches to addressing some of these challenges. The creation of lines that enable ratiometric measurements ($Acta2^{BAC}$-mCherry and $Acta2^{BAC}$-Vermilion; Fig. 4) add additional experimental advantages in this regard. Similarly, the ability to initiate synthesis of critical smooth muscle second messengers through the expression of light sensitive chimeric receptor proteins fused to catalytic domains of $\alpha$1 and ß2 adrenoceptors[8] provides important capabilities to probe vascular control mechanisms in smooth muscle tissues, and the ability to control the synthesis in an individual cell type.

Finally, we report additional lines that enable studies of sympathetic neurons, glial cells, and Type II alveolar cells. These lines show robust, tissue -specific expression of the optoeffector or optosensor proteins, enabling similar studies of neurovascular and lung cell signaling.

In summary, BAC transgenic optogenetic effector and sensor lines provide novel experimental platforms for real-time *in vivo* investigations of molecular signaling in complex physiological systems. The mice are available to experimenters through JAX and represent a tool kit that can advance the use of optogenetics in a wide array of experimental investigations.

## References


1. Tsien RY. Breeding molecules to spy on cells. *Harvey Lect*. 2003;99:77-93.
2. Kotlikoff MI. Genetically encoded Ca2+ indicators: using genetics and molecular design to understand complex physiology. *J Physiol*. 2007;578:55-67.
3. Fenno L, Yizhar O and Deisseroth K. The development and application of optogenetics. *AnnuRevNeurosci*. 2011;34:389-412.
4. Akerboom J, Carreras Calderon N, Tian L, Wabnig S, Prigge M, Tolo J, Gordus A, Orger MB, Severi KE, Macklin JJ, Patel R, Pulver SR, Wardill TJ, Fischer E, Schuler C, Chen TW, Sarkisyan KS, Marvin JS, Bargmann CI, Kim DS, Kugler S, Lagnado L, Hegemann P, Gottschalk A, Schreiter ER and Looger LL. Genetically encoded calcium indicators for multi-color neural activity imaging and combination with optogenetics. *Frontiers in molecular neuroscience*. 2013;6:2.
5. Gengyo-Ando K, Kagawa-Nagamura Y, Ohkura M, Fei X, Chen M, Hashimoto K and Nakai J. A new platform for long-term tracking and recording of neural activity and simultaneous optogenetic control in freely behaving Caenorhabditis elegans. *J Neurosci Methods*. 2017;286:56-68.
6. Zariwala HA, Borghuis BG, Hoogland TM, Madisen L, Tian L, De Zeeuw CI, Zeng H, Looger LL, Svoboda K and Chen TW. A Cre-dependent GCaMP3 reporter mouse for neuronal imaging in vivo. *JNeurosci*. 2012;32:3131-3141.
7. Tallini YN, Shui B, Greene KS, Deng KY, Doran R, Fisher PJ, Zipfel W and Kotlikoff MI. BAC transgenic mice express enhanced green fluorescent protein in central and peripheral cholinergic neurons. *Physiol Genomics*. 2006;27:391-397.
8. Airan RD, Thompson KR, Fenno LE, Bernstein H and Deisseroth K. Temporally precise in vivo control of intracellular signalling. *Nature*. 2009;458:1025-1029.
9. Zhang F, Wang LP, Boyden ES and Deisseroth K. Channelrhodopsin-2 and optical control of excitable cells. *NatMethods*. 2006;3:785-792.
10. Jesty SA, Steffey MA, Lee FK, Breitbach M, Hesse M, Reining S, Lee JC, Doran RM, Nikitin AY, Fleischmann BK and Kotlikoff MI. c-kit+ precursors support postinfarction myogenesis in the neonatal, but not adult, heart. *ProcNatlAcadSciUSA*. 2012.
11. Prada MP, Syed AU, Buonarati OR, Reddy GR, Nystoriak MA, Ghosh D, Simo S, Sato D, Sasse KC, Ward SM, Santana LF, Xiang YK, Hell JW, Nieves-Cintron M and Navedo MF. A Gs-coupled purinergic receptor boosts Ca(2+) influx and vascular contractility during diabetic hyperglycemia. *Elife*. 2019;8.
12. Fernandez JA, Bankhead P, Zhou H, McGeown JG and Curtis TM. Automated detection and measurement of isolated retinal arterioles by a combination of edge enhancement and cost analysis. *PloS one*. 2014;9:e91791.
13. Jones JS, Small DM and Nishimura N. In Vivo Calcium Imaging of Cardiomyocytes in the Beating Mouse Heart With Multiphoton Microscopy. *Front Physiol*. 2018;9:969.
14. Allan-Rahill NH, Lamont MRE, Chilian WM, Nishimura N and Small DM. Intravital Microscopy of the Beating Murine Heart to Understand Cardiac Leukocyte Dynamics. *Front Immunol*. 2020;11:92.

15. Pologruto TA, Sabatini BL and Svoboda K. ScanImage: flexible software for operating laser scanning microscopes. *Biomed Eng Online*. 2003;2:13.
16. Bagher P and Segal SS. The mouse cremaster muscle preparation for intravital imaging of the microcirculation. *Journal of visualized experiments : JoVE*. 2011.
17. Moosmang S, Stieber J, Zong X, Biel M, Hofmann F and Ludwig A. Cellular expression and functional characterization of four hyperpolarization-activated pacemaker channels in cardiac and neuronal tissues. *Eur J Biochem*. 2001;268:1646-52.
18. DiFrancesco D. Pacemaker mechanisms in cardiac tissue. *Annu Rev Physiol*. 1993;55:455-72.
19. Tallini YN, Ohkura M, Choi BR, Ji G, Imoto K, Doran R, Lee J, Plan P, Wilson J, Xin HB, Sanbe A, Gulick J, Mathai J, Robbins J, Salama G, Nakai J and Kotlikoff MI. Imaging cellular signals in the heart in vivo: Cardiac expression of the high-signal Ca2+ indicator GCaMP2. *Proceedings of the National Academy of Sciences of the United States of America*. 2006;103:4753-8.
20. Gulick J, Subramaniam A, Neumann J and Robbins J. Isolation and characterization of the mouse cardiac myosin heavy chain genes. *The Journal of biological chemistry*. 1991;266:9180-5.
21. Mack CP and Owens GK. Regulation of smooth muscle alpha-actin expression in vivo is dependent on CArG elements within the 5' and first intron promoter regions. *Circulation research*. 1999;84:852-61.
22. Bethge P, Carta S, Lorenzo DA, Egolf L, Goniotaki D, Madisen L, Voigt FF, Chen JL, Schneider B, Ohkura M, Nakai J, Zeng H, Aguzzi A and Helmchen F. An R-CaMP1.07 reporter mouse for cell-type-specific expression of a sensitive red fluorescent calcium indicator. *PloS one*. 2017;12:e0179460.
23. Johnson RP, El-Yazbi AF, Hughes MF, Schriemer DC, Walsh EJ, Walsh MP and Cole WC. Identification and functional characterization of protein kinase A-catalyzed phosphorylation of potassium channel Kv1.2 at serine 449. *The Journal of biological chemistry*. 2009;284:16562-74.
24. Luykenaar KD and Welsh DG. Activators of the PKA and PKG pathways attenuate RhoA-mediated suppression of the KDR current in cerebral arteries. *American journal of physiology Heart and circulatory physiology*. 2007;292:H2654-63.
25. Wellman GC, Santana LF, Bonev AD and Nelson MT. Role of phospholamban in the modulation of arterial Ca(2+) sparks and Ca(2+)-activated K(+) channels by cAMP. *Am J Physiol Cell Physiol*. 2001;281:C1029-37.
26. Nelson MT and Quayle JM. Physiological roles and properties of potassium channels in arterial smooth muscle. *Am J Physiol*. 1995;268:C799-822.
27. Straub AC, Zeigler AC and Isakson BE. The myoendothelial junction: connections that deliver the message. *Physiology (Bethesda)*. 2014;29:242-9.
28. Tallini YN, Brekke JF, Shui B, Doran R, Hwang SM, Nakai J, Salama G, Segal SS and Kotlikoff MI. Propagated endothelial Ca2+ waves and arteriolar dilation in vivo: measurements in Cx40BAC GCaMP2 transgenic mice. *Circulation research*. 2007;101:1300-9.
29. Welsh DG and Segal SS. Endothelial and smooth muscle cell conduction in arterioles controlling blood flow. *Am J Physiol*. 1998;274:H178-86.

30. Delorme B, Dahl E, Jarry-Guichard T, Marics I, Briand JP, Willecke K, Gros D and Theveniau-Ruissy M. Developmental regulation of connexin 40 gene expression in mouse heart correlates with the differentiation of the conduction system. *Dev Dyn*. 1995;204:358-71.
31. Gonzalez-Lopez E and Vrana KE. Dopamine beta-hydroxylase and its genetic variants in human health and disease. *Journal of neurochemistry*. 2020;152:157-181.
32. Nakai J and Ohkura M. Probing calcium ions with biosensors. *Biotechnol Genet Eng Rev*. 2003;20:3-21.
33. Madisen L, Zwingman TA, Sunkin SM, Oh SW, Zariwala HA, Gu H, Ng LL, Palmiter RD, Hawrylycz MJ, Jones AR, Lein ES and Zeng H. A robust and high-throughput Cre reporting and characterization system for the whole mouse brain. *Nature neuroscience*. 2010;13:133-40.
34. Ohkura M, Sasaki T, Sadakari J, Gengyo-Ando K, Kagawa-Nagamura Y, Kobayashi C, Ikegaya Y and Nakai J. Genetically encoded green fluorescent Ca2+ indicators with improved detectability for neuronal Ca2+ signals. *PloS one*. 2012;7:e51286.
35. Tian L, Hires SA, Mao T, Huber D, Chiappe ME, Chalasani SH, Petreanu L, Akerboom J, McKinney SA, Schreiter ER, Bargmann CI, Jayaraman V, Svoboda K and Looger LL. Imaging neural activity in worms, flies and mice with improved GCaMP calcium indicators. *Nature methods*. 2009;6:875-81.
36. Mond HG and Proclemer A. The 11th world survey of cardiac pacing and implantable cardioverter-defibrillators: calendar year 2009--a World Society of Arrhythmia's project. *Pacing Clin Electrophysiol*. 2011;34:1013-27.
37. Vedantham V. New Approaches to Biological Pacemakers: Links to Sinoatrial Node Development. *Trends in molecular medicine*. 2015;21:749-761.
38. Meyers JD, Jay PY and Rentschler S. Reprogramming the conduction system: Onward toward a biological pacemaker. *Trends in cardiovascular medicine*. 2016;26:14-20.
39. Nyns ECA, Poelma RH, Volkers L, Plomp JJ, Bart CI, Kip AM, van Brakel TJ, Zeppenfeld K, Schalij MJ, Zhang GQ, de Vries AAF and Pijnappels DA. An automated hybrid bioelectronic system for autogenous restoration of sinus rhythm in atrial fibrillation. *Science translational medicine*. 2019;11.
40. Bui AL, Horwich TB and Fonarow GC. Epidemiology and risk profile of heart failure. *Nat Rev Cardiol*. 2011;8:30-41.
41. Asimaki A, Kleber AG, MacRae CA and Saffitz JE. Arrhythmogenic Cardiomyopathy - New Insights into Disease Mechanisms and Drug Discovery. *Prog Pediatr Cardiol*. 2014;37:3-7.
42. Nakamura K and Murry CE. Function Follows Form- A Review of Cardiac Cell Therapy. *Circ J*. 2019;83:2399-2412.
43. Duncker DJ and Bache RJ. Regulation of coronary blood flow during exercise. *Physiological reviews*. 2008;88:1009-86.
44. Sonkusare SK, Dalsgaard T, Bonev AD, Hill-Eubanks DC, Kotlikoff MI, Scott JD, Santana LF and Nelson MT. AKAP150-dependent cooperative TRPV4 channel gating is central to endothelium-dependent vasodilation and is disrupted in hypertension. *Sci Signal*. 2014;7:ra66.

45. Sonkusare SK, Bonev AD, Ledoux J, Liedtke W, Kotlikoff MI, Heppner TJ, Hill-Eubanks DC and Nelson MT. Elementary Ca2+ signals through endothelial TRPV4 channels regulate vascular function. *Science*. 2012;336:597-601.
46. Gonzales AL, Klug NR, Moshkforoush A, Lee JC, Lee FK, Shui B, Tsoukias NM, Kotlikoff MI, Hill-Eubanks D and Nelson MT. Contractile pericytes determine the direction of blood flow at capillary junctions. *Proceedings of the National Academy of Sciences of the United States of America*. 2020;117:27022-27033.

**Figure 1. Illustration of an experiment with multiallelic CHROMus™ mice**. In this illustration, a biallelic SA nodal CatCh2/cardiomyocyte-GCaMP8 mouse is generated to study the response of cardiac cycle and cardiomyocytes to the activation of the sinoatrial node with an external stimulation, a blue laser pulse. The SA nodal tissue is activated with blue laser delivered by a fiber optic filament and the response of intracellular calcium in cardiomyocytes is monitored by GCaMP8 fluorescence and the pacing ECG recorded. LA – left atrium, RA – right atrium, RV – right ventricle, LV – left ventricle, Ao – aorta, SVC – superior vena cava, SAN – sinoatrial node. Figure adapted from Virginia Miller.

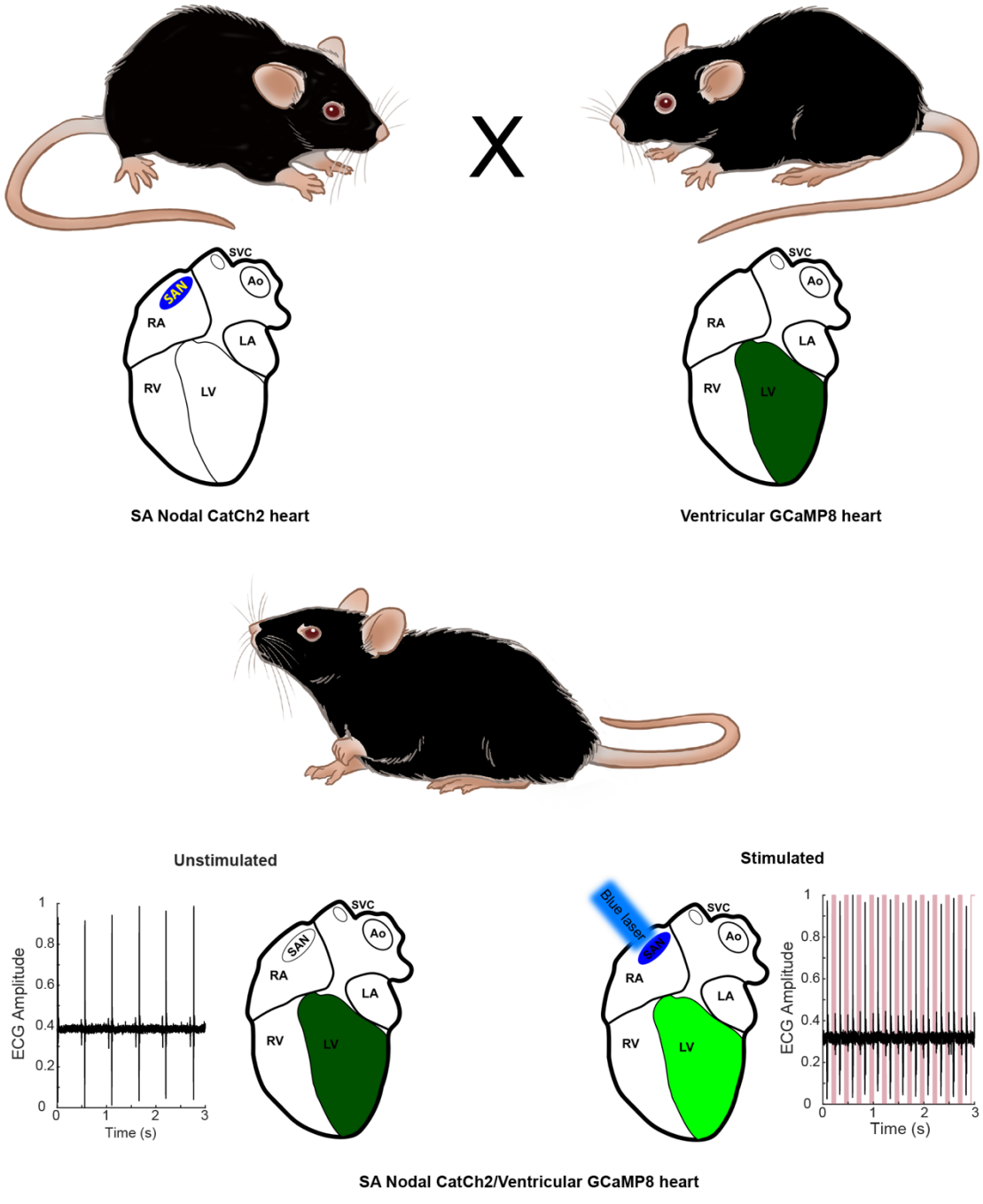

**Figure 2. HCN4$^{BAC}$- CatCh2_IRES_LacZ and HCN4$^{BAC}$-GCaMP8 strains express the transgenic LacZ protein and fluorescent calcium reporter protein GCaMP8. A**, X-gal staining of HCN4$^{BAC}$-CatCh2_IRES_LacZ adult heart detected LacZ expression in the SA node, AV junction and the ventricular conductance network (arrows). Scale bars – upper panel, 2 mm, lower panels, 300 μm. **B**, Left panel – X-gal staining of wildtype and HCN4$^{BAC}$-CatCh2_IRES_LacZ E10.5 embryos; upper images – whole embryo, lower images – cardiac region. Right panel – Whole heart X-gal staining of neonatal heart showing staining in the cardiac conductance system including the SA nodal region, atrioventricular junction and the ventricle chambers. **C**, ECG recording in an anesthetized HCN4$^{BAC}$-CatCh2_IRES_LacZ mouse during intravital pacing with laser illumination. ECG recordings from laser stimulation of transgenic CatCh2 protein demonstrate pacing from 2 to 4 Hz (3 Hz not shown) but not at 5 Hz. **D**, ECG averaged by aligning R-wave peaks during laser-stimulated and unstimulated beats (shading indicates standard deviation, n = 273 stimulated beats, n = 115 unstimulated beats from same mouse (same as in E), dark and light gray indicate average and standard deviation of laser pulse onset and offset times). Laser power is 32.2 mW, pulse length is 70 ms. **E**, R-wave duration in stimulated and unstimulated beats (****: $p < 0.001$, Mann-Whitney test). Solid lines and dashed lines show median and quartiles. **F**, Averaged ECG aligned by P-wave peak during stimulated and unstimulated beats. **G**, Quantification of PR interval duration shows elongation in stimulated compared to unstimulated beats (****: $p < 0.001$, Mann-Whitney test). **H**, Fluorescent calcium measurement during optical stimulation of SA nodal tissue in *HCN4$^{BAC}$*-CatCh2_IRES_LacZ /*αMHC*-GCaMP8 perfused mouse heart at 2 Hz shows pacing of the cardiac contraction cycle. **Top**, fluorescent images from the left ventricle with timing of laser pulses indicated by red box. **Bottom**, a plot of the GCaMP8 intensity from the left ventricle in the outlined box (left image). Scale bar – 200 μm. **I**, Expression of GCaMP8 protein in embryonic and adult heart from HCN4$^{BAC}$-GCaMP8 strain. Left, anti-GFP immunostaining of paraffin section from E13.5 embryo. Scale bars – 2 mm and 200 μm; right, dorsal view of an adult heart showing native GCaMP8 fluorescence in the SA nodal region, the right carotid vein and the base of common carotid vein. RA - right atrium, CCV - common carotid vein, RCV - right carotid vein, LV - left ventricle, and RV - right ventricle.

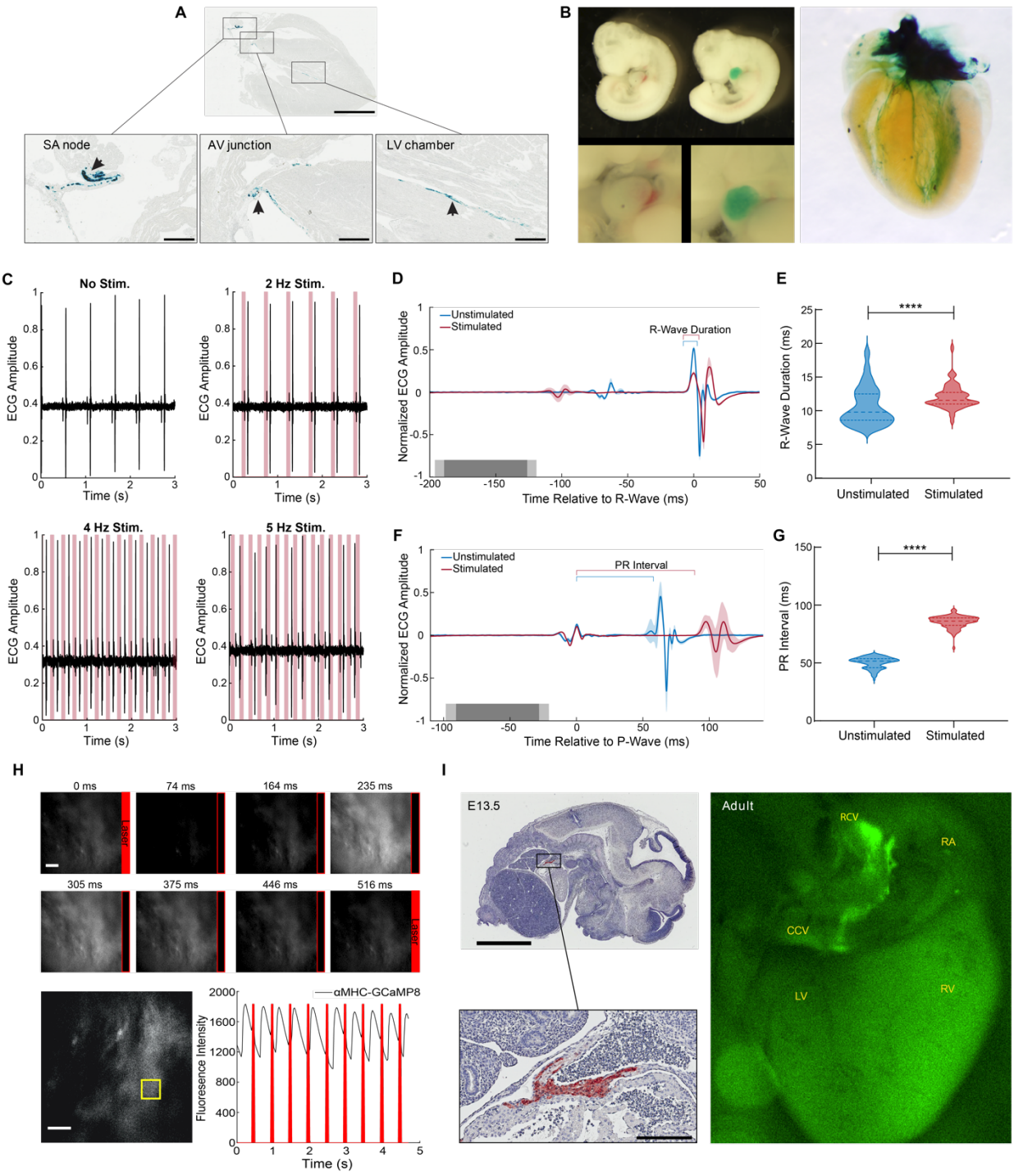

**Figure 3. Analysis of transgene expression and activity in αMHC-CatCh2_IRES_LacZ and αMHC-GCaMP8 strains. A**, X-gal staining of cardiomyocytes in αMHC-CatCh2_IRES_LacZ, scale bar – 200 and 60 μm. **B**, ECG recording during intravital laser stimulation of the CatCh2 protein in the left ventricle at various frequencies (laser power is 32.2 mW, average pulse length is 14 ms). **C**, R-wave centered average of all stimulated and unstimulated beats shows R-wave widening (shading indicates standard deviation of ECG signal, dark and light gray indicate average and standard deviation of laser pulse onset and offset times). **D**, The R-wave durations with and without laser stimulation of the transgenic CatCh2 protein are shown from three different mice. **E**, ECG recordings demonstrating the transition from the autonomous conduction cycle to laser-stimulated conduction and **F**, the use of laser stimulation of the αMHC-CatCh2 mouse ventricle to cause a premature ventricular contraction. **G,** Expression of GCaMP8 in heart of an adult αMHC-GCaMP8 mouse; **top**, native fluorescence, **bottom**, anti-GFP immunohistochemistry, scale bars - 200 μm. **H**, Intravital two-photon microscopy of the αMHC-GCaMP8 heart. Frames from a three-dimensional reconstruction of $\alpha MHC^{BAC}$-GCaMP8 fluorescence over a cardiac cycle. Each frame represents a 10 % increment of the cardiac cycle defined by the peak of the R-wave. The x-axis is the anterior to posterior direction, the y-axis is the apex to base direction, and the z-axis is the epicardium to endocardium direction of the left ventricle free wall. A 166 x 166 x 100 μm (xyz) region is shown. GCaMP8 fluorescence in cardiomyocytes is shown in green and the vasculature labeled with Texas Red conjugated dextran is shown in magenta. **I**, Average and standard deviation of change in fluorescence intensity of the imaged region demonstrating calcium transients during the cardiac cycle.

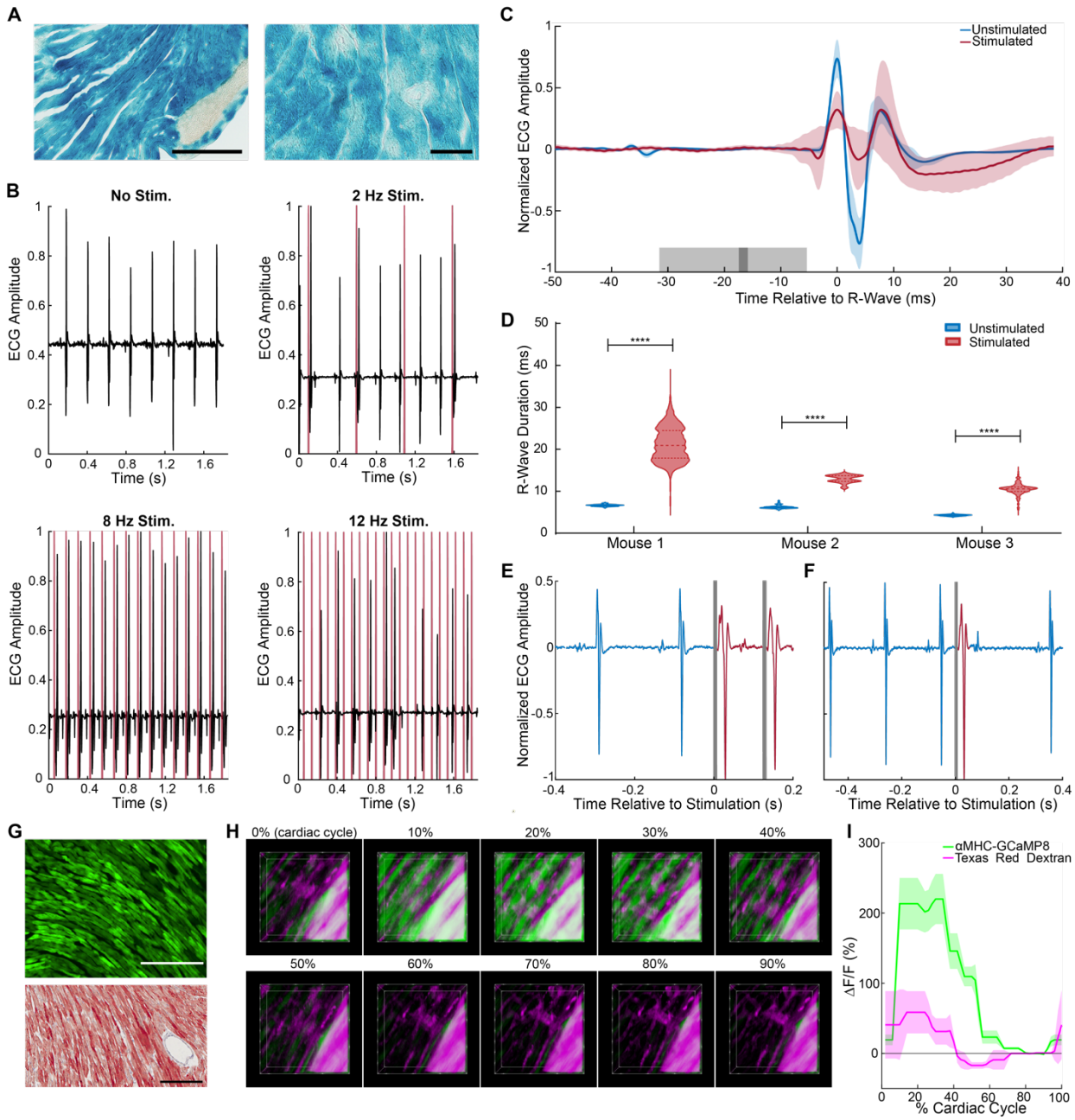

**Figure 4. Analysis of transgene expression in Acta2$^{BAC}$ reporter strains**. **A,** Native fluorescence of surface blood vessels from Acta2$^{BAC}$-GCaMP5_mCherry (upper) and Acta2$^{BAC}$-GCaMP8.1_mVermilion brain (lower). Note the absence of fluorescence in veins (arrows). Left panel -overlay, right panels – red and green channels. **B,** X-gal staining of brain surface arteries from Acta2 optoeffector strains. All images shown are representative images from 3 animals unless otherwise specified.

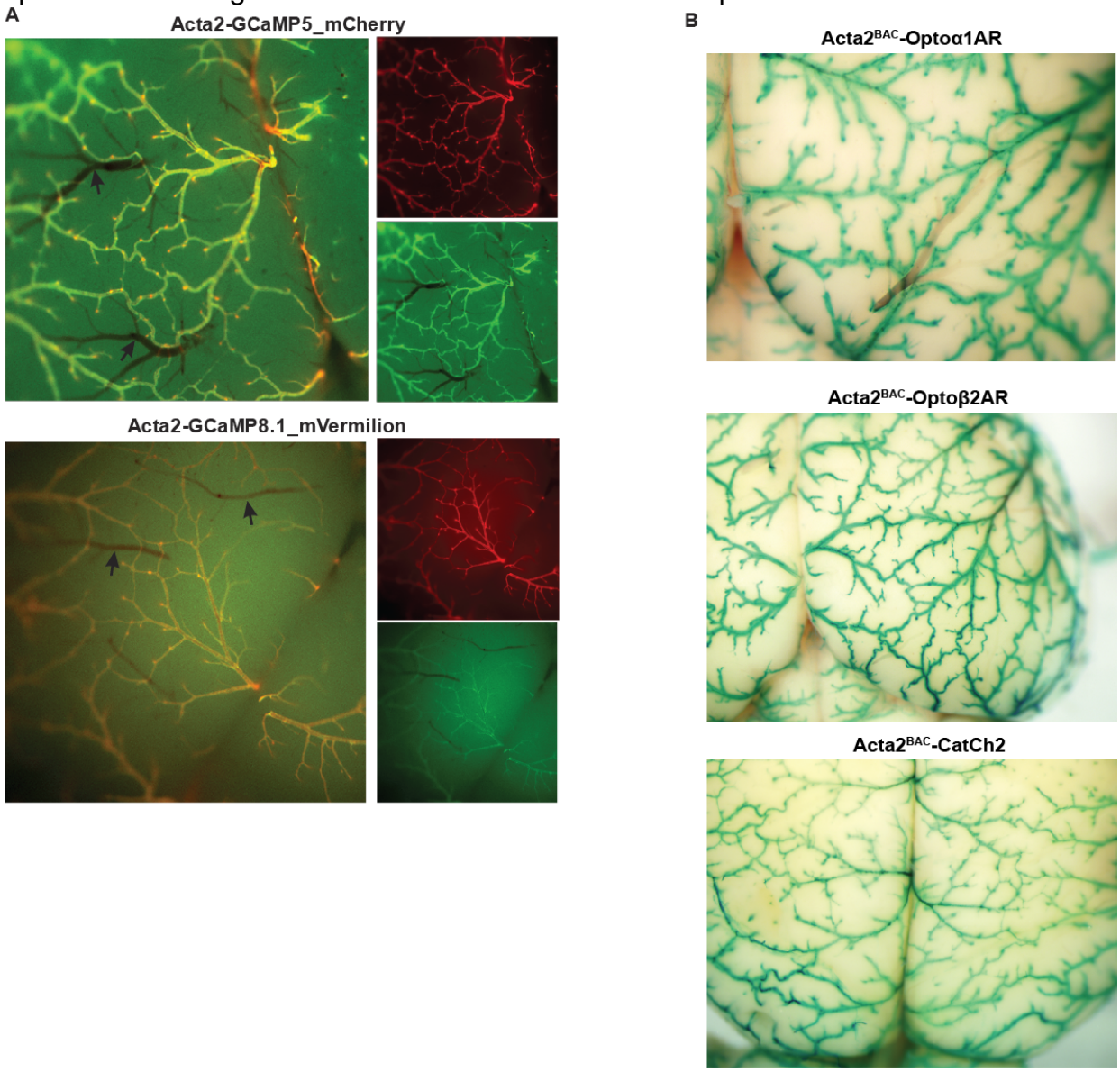

**Figure 5. Analysis of transgene activity in Acta2$^{BAC}$ effector strains**. **A,** Biological activity of Acta2$^{BAC}$ effector strains. The activation of optogenetic proteins in the effector strains results in either vessel contraction (Acta2$^{BAC}$-Opto$\alpha$1AR_IRES_LacZ – left panel, Acta2$^{BAC}$-CatCh2_IRES_LacZ –right panel) or relaxation (Acta2$^{BAC}$-Optoß2AR_IRES_LacZ – middle panel). **B,** Laser activation of transgenic Optoß2AR proteins induces K currents in isolated arterial myocytes. Upper panel – mesenteric myocytes, lower panel –cerebral myocytes. **C,** Laser activation of transgenic CatCh2 protein induces inward membrane current. Upper panel – repeated laser pulses result in rapid inward current in cerebral myocytes. Middle panels – long pulses achieve a steady state inward current in cerebral (upper) and mesenteric myocytes (lower) after an initial spike only on the first pulse. Bottom panel – activation of cerebral myocytes results in higher initial and steady state current compared to mesenteric myocytes. The Optoß2AR data were derived from 5 cells isolated from 3 mice and the CatCh2 data were generated from 8 cells isolated from 5 mice.

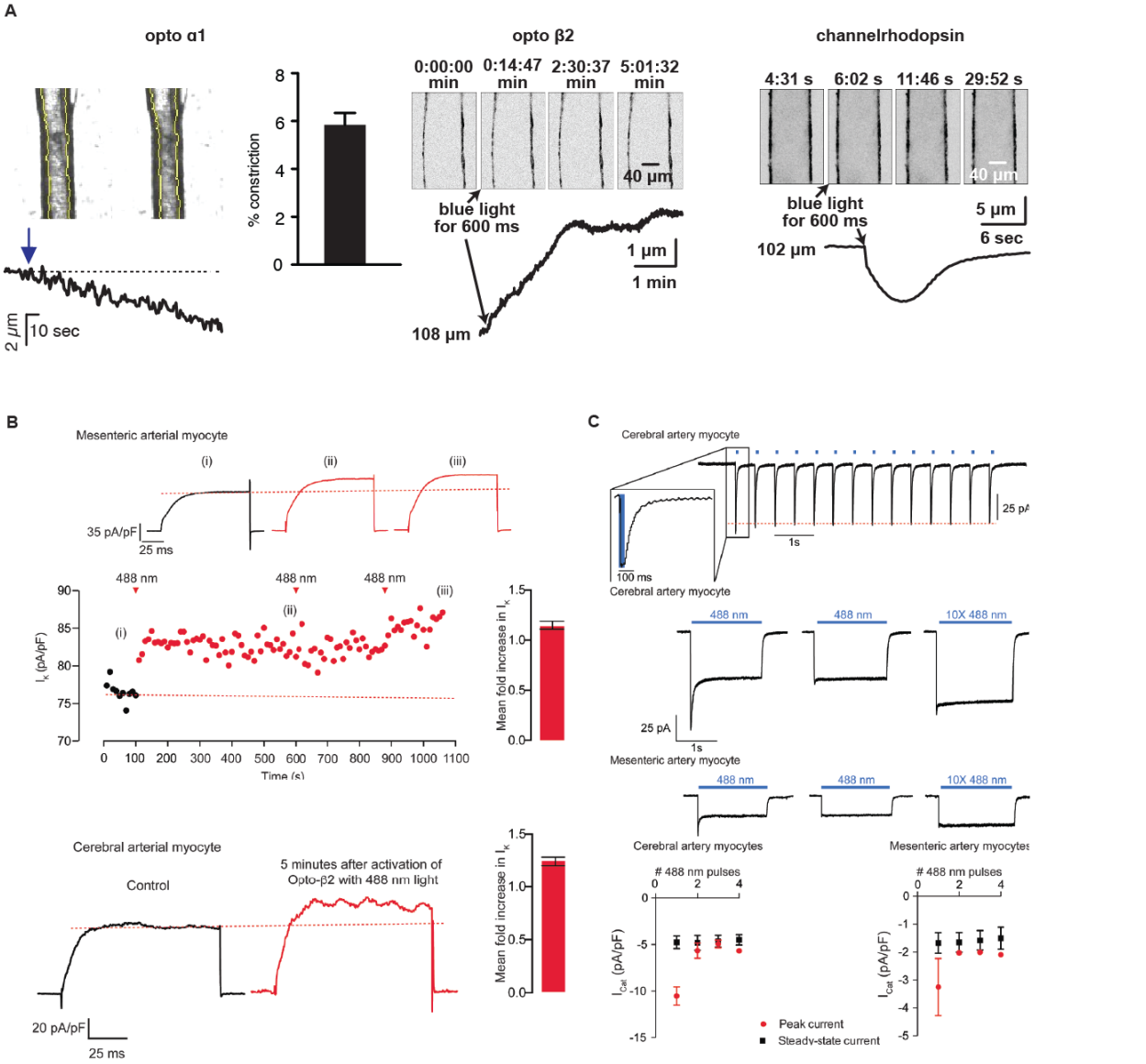

**Figure 6. Analysis of optogenetic protein expression in Cdh5BAC strains**. **A,** X-gal staining of heart cryosections from Cdh5$^{BAC}$-Opto$\alpha$1AR_IRES_LacZ, Cdh5$^{BAC}$-Opto$\beta$2AR_IRES_LacZ and Cdh5$^{BAC}$-CatCh2_IRES_LacZ mice. Scale bars - 200 microns. **B,** Native fluorescence of GCaMP8 protein in heart cryosection (left panel) and brain dorsal surface (right panel). Scale bar - 200 µm. **C,** Intravital 2-photon imaging of Cdh5 $^{BAC}$-GCaMP8 mice shows endothelial GCaMP8 (green) labelling of coronary microvasculature. Intravenous Texas-Red conjugated 70-kDa dextran identifies the vessel lumen (magenta). All images shown are representative images from 3 animals unless otherwise specified.

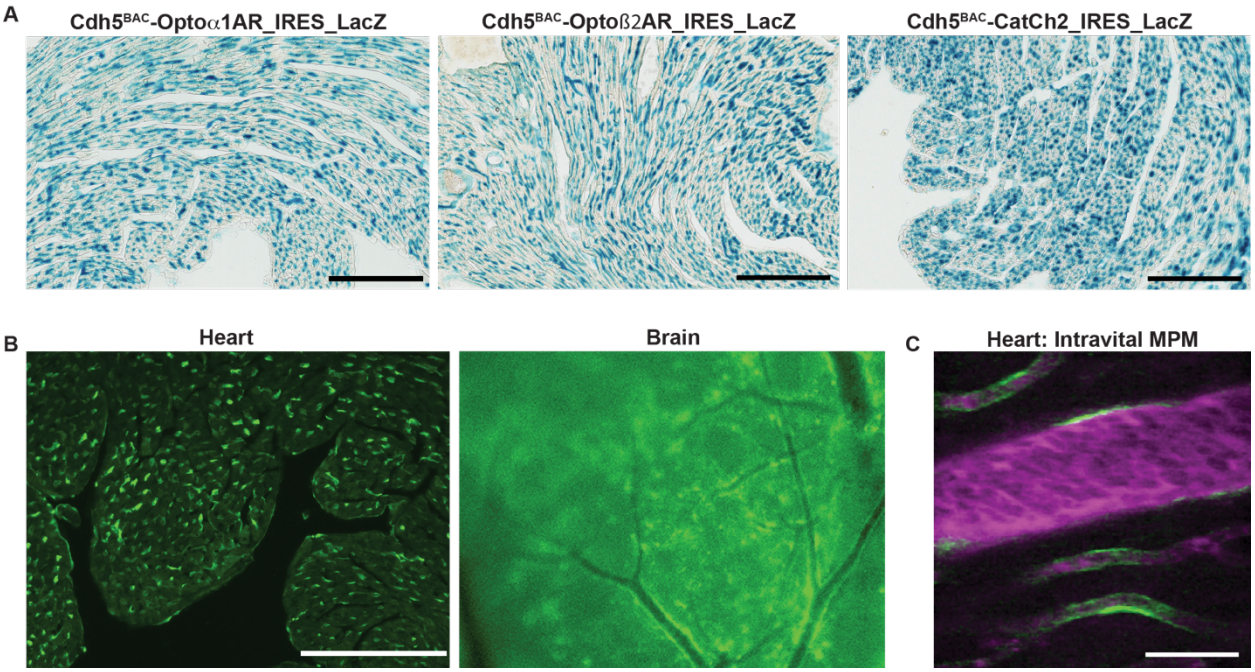

**Figure 7. Effector proteins in Cdh5$^{BAC}$-Optoα1AR_IRES_LacZ and Cdh5$^{BAC}$-Optoß2AR_IRES_LacZ strains are biologically active**. **A,** Laser stimulation of femoral artery in Cdh5$^{BAC}$-Optoα1AR induces vasodilation. Left panel – MATLAB generated 3D rendering of vessel width and intensity over time. The arrowheads mark the start and end of laser activation and the asterisk marks dilation of the artery. Right panel – Comparison of peak change in vessel width between Cdh5$^{BAC}$-Optoα1AR-_IRES_LacZ and C57BL6 control mice, n=3 both groups. **B,** Activation of Optoα1AR protein results in migration of vasodilation away from the laser irradiation point. Left panel – bright field image of the femoral artery with positions of the mid, right (Rt) and left (Lf) analysis positions indicated. Red dashed circle outlines the laser irradiation spot on the vessel. Right panel – graph plotting the net change in vessel width over time. **C,** Vessel relaxation is dependent on laser intensity. **D,** Comparison of vasodilation induced by Optoα1AR and Optoß2AR proteins with laser power at 32.2 mW.

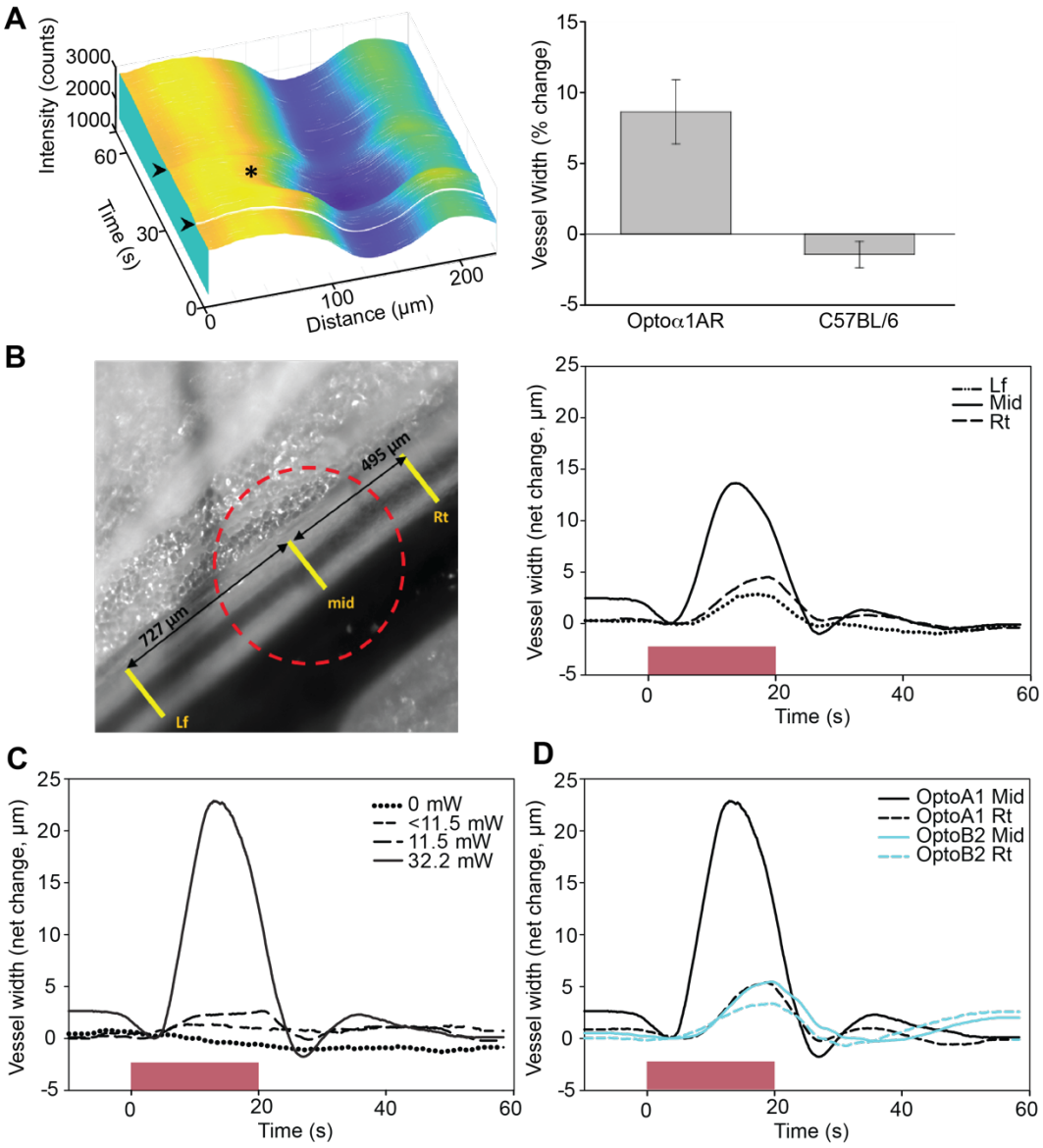

**Figure 8. Characterization of other CHROMus™ strains. A,** Anti-GFP IHC of Cx40$^{BAC}$-GCaMP5_mCherry mouse. GCaMP5 is expressed in the atrioventricular junction (AVJ) region, atrial myocytes (AM) (left panel) and cells lining the endocardium in the adult heart (middle panel; scale bars – 200μm) and the renal artery (right panel; scale bar – 60μm). **B,** X-gal staining of adult brain sagittal section from Dbh$^{BAC}$-CatCh2_IRES_lacZ mouse showing LacZ expression in the *locus coeruleus* region. Box outlines area of enlargement. CB – cerebellum, LC – *locus coeruleus*. Scale bars; top panel - 500μm, bottom panel - 200μm. **C,** X-gal staining of cerebellar region from Aldh1L1$^{BAC}$-Opto$\alpha$1AR_IRES_LacZ mouse. Box outlines area of enlargement. Scale bars; top panel -2mm, bottom panel – 200μm. All images shown are representative images from 3 animals unless otherwise specified.